Journal of Molecular Liquids 254 (2018) 433–445

Contents lists available at ScienceDirect

Journal of Molecular Liquids

journal homepage: www.elsevier.com/locate/molliq

Adsorption behaviors of hazardous methylene blue and hexavalent chromium on novel materials derived from *Pterospermum acerifolium* shells

S. Rangabhashiyam *, P. Balasubramanian *

Department of Biotechnology and Medical Engineering, National Institute of Technology Rourkela, Odisha 769 008, India

ARTICLE INFO

Article history:
Received 9 November 2017
Received in revised form 11 January 2018
Accepted 23 January 2018

Keywords:
Adsorption
Pterospermum acerifolium shells
Methylene blue
Hexavalent chromium
Pre-treatment

ABSTRACT

Heavy metal and dye are diffused pollutants in the wastewater, which impose a serious threat to the environment. Adsorption is the unconventional technique used for the sequestration of wastewater contaminants. Adsorbents prepared from *Pterospermum acerifolium* shells were successfully used for the first time for removing methylene blue and hexavalent chromium from aqueous solutions in a batch system. The effect of sulfuric acid, phosphoric acid treatments on *Pterospermum acerifolium* shells (SPAS, PPAS) and its native form (PAS) was investigated on the adsorption process. The influences of the solution pH (2.0–10.0), adsorbent dosage (0.01–0.1 g), initial MB, Cr(VI) concentrations (50–250 mg/L), and temperature (303−323 K) were examined for the removal process. Thermodynamic parameters were estimated for the thermodynamical modeling of the adsorption processes. Langmuir isotherm model better described the MB and Cr(VI) removal process. The maximum adsorption capacity achieved was 125 mg/g (PAS), 166.66 mg/g (SPAS), and 250 mg/g (PPAS) for MB removal and for Cr(VI) was 76.92 mg/g (PAS), 142.85 mg/g (SPAS), and 111.11 mg/g (PPAS), respectively. The experimental data as a function of contact time was modeled using the adsorption kinetic equations of pseudo-first order, pseudo-second order, Elovich and intra-particle diffusion models. The experimental adsorption data best correlated to pseudo-second order model. The shells of *Pterospermum acerifolium* are an efficient precursor for the preparation of adsorbents (PAS, SPAS, PPAS), successfully applied for the removal of methylene blue and hexavalent chromium from aqueous solutions.

1. Introduction

Till recent years, water pollution due to organic and inorganic compounds is rising rapidly because of industrial effluents discharged into the environment without treatment [1]. Dyes are widely used as a vital raw material for colorants in textiles, rubber, plastics, paper, leather, cosmetics, printing, food, and pharmaceutical industries. About 10% of dye substances in the form of waste were discharged as colored industrial effluent after manufacturing processes and various industrial operations [2,3]. More than 10,000 dyestuffs were produced annually and above 700,000 metric tons of dyes are available commercially worldwide [4]. The discharge of untreated colored effluent into the water bodies causes environmental issues such as oxygen content depletion in water and reduced sunlight penetration, which put the life of aquatic animals and plants in danger. Moreover, the industrial wastewater containing dyes is mostly associated with poisonous and carcinogenic effect to the human beings [5]. Potable water contamination with dyes even with a concentration of 1.0 mg/L could cause significant color impact and make unfit for human consumption [6]. Dye is a colored organic substance, which provides color to diverse substrates. Based on the ionic charge distribution on the dye molecules, they are broadly categorized into anionic, cationic, and non-ionic. Compared to anionic dyes, toxicity effects are higher in cationic dyes [7].

Methylene blue belongs to the category of cationic dye and has a heterocyclic aromatic structure. Being the commercial dye with high volume production, Methylene blue finds its applications in coloring paper, hair colorant, dyeing cotton, wools, paper stock coating, etc. Used as a staining agent in the body fluids and tissues, this helps for an easier view during operations and diagnostic assessment. Methylene blue is also used in the medical treatment of methaemoglobinemia and cyanide poisoning [8,9]. Irrespective of the broader applications, this dye has a number of harmful effects on living systems. Methylene blue causes headache, eye burns, breathing difficulties, increased heart rate, chest pain, burning sensation in mouth, nausea, vomiting, diarrhea, gastritis, more sweating, shock, mental confusion, jaundice, Heinz body formation, cyanosis, quadriplegia, and tissue necrosis [10,11].

Heavy metals are highly persistent, bioaccumulative, and most toxic in nature. Chromium is one of the toxic heavy metals listed in top 20

* Corresponding authors.
E-mail addresses: rambhashiyam@gmail.com (S. Rangabhashiyam), biobala@nitrkl.ac.in (P. Balasubramanian).

https://doi.org/10.1016/j.molliq.2018.01.131
0167-7322/

contaminants under the category of hazardous materials. Many industrial processes such as aluminum, electroplating, fertilizer, leather tanning, steel, textile mill, paint, dye, etc., generate effluent with high chromium concentration. The chromium concentrations in the spent chrome liquors and tanneries waste are 2900–4500 mg/L and 10–50 mg/L, respectively. Chromium usually exists in the aqueous environment as Cr(III) and Cr(VI) forms. Relatively, Cr(III) is harmless, immobile and the trace concentration of Cr(III) plays a vital role in the glucose metabolism. Whereas, Cr(VI) associated with the property of mobility, acts as a strong oxidizing agent consequent to carcinogenic and mutagenic diseases. The health problems in humans due to the hazardous effects of Cr(VI) include dermatitis, skin irritation, hemorrhage, epigastric pain, bronchitis, chronic ulcers, nasal septum perforation, lung cancer, pneumonitis, and liver inflammation [12–14]. The maximum permissible levels for Cr(VI) in the potable, inland surface and industrial effluent are 0.05, 0.1, and 0.25 mg/L, respectively [15]. Adsorption is one of the most widely used cutting-edge technique for removing wastewater pollutants due to its simple design, ease of operation, economic efficiency, insensitivity to toxic contaminants, and highly selective capacity even at the low pollutant concentration [16,17]. Activated carbon is the most commonly used adsorbent for effluent treatment in the industrial scale. Activated carbon exhibits the characteristic features of higher surface area, porous structure, variable surface chemistry properties, and higher mechanical strength [18]. Nevertheless, most of the commercial activated carbons are produced using coal, which is not an economical and non-renewable material. Recently, more research is focused on the employment of cheap and efficient precursors such as agricultural wastes, low-grade plants, forest residues, and industrial by-products for the preparation of activated carbons. Among these precursors, lignocellulosic source materials are used in largest for the activated carbon production [19,20].

The *Pterospermum acerifolium* is a shrub that belongs to the Sterculiaceae family, commonly distributed in the Southeast Asia and particularly found in the region of sub-Himalaya, on the outside Himalayan valley and present in the hills up to 4000 ft. [21]. The common names of the *Pterospermum acerifolium* plant are Muchukunda, Karnikara, Matsakanda, and Kanakchampa. In traditional Indian medicine, *Pterospermum acerifolium* plant is used for the treatment of leucorrhoea, smallpox, leprosy, haemostasis, ulcer, anti-inflammation, and tumors [22]. The present study is dedicated to use native and acids-modified *Pterospermum acerifolium* shells for the first time for the removal of Methylene blue and hexavalent chromium from aqueous solutions. The adsorbents were characterized using Fourier Transform Infrared Spectroscopy (FT-IR) and Environmental Scanning Electron Microscopy (E-SEM). The parameters of the adsorption system were optimized to attain the maximum removal efficiency of Methylene blue and hexavalent chromium. The adsorption process mechanisms were examined by fitting the experimental data to isotherms and kinetic models.

2. Materials and methods

2.1. Preparation of the adsorbents and characterizations

The *Pterospermum acerifolium* shells were collected from the suburbs of the Rourkela city in Odisha, India. The shells were washed with distilled water and dried at 110 °C for 1 h. The dried and cleaned precursor was subjected to ground, sieved to the size range of 100–200 μm (PAS). The chemical pretreatment was carried out through sulfuric acid and phosphoric acid separately. The first method of sulfuric acid modification was done using 98% sulfuric acid 1:2 (g PAS/g H_2SO_4), the pretreated biomass was allowed for carbonization at the temperature of 150 °C for 24 h in a hot air oven. The carbonized material was washed using distilled water and then soaked in 1% sodium bicarbonate solution for 24 h. The prepared samples were washed with distilled water and finally oven dried at 105 °C for 24 h (SPAS). The second method of acid activation was performed using 88% phosphoric acid at a ratio of 1:2.5 (g PAS/g H_3PO_4) and then oven dried at 110 °C for 3 h. The samples were transferred into a muffle furnace and carbonized at the temperature of 400 °C and the activation time duration was 1.5 h. The carbonized samples were treated with 1% sodium bicarbonate, followed by drying at 105 °C for 24 h (PPAS). The prepared adsorbents of the *Pterospermum acerifolium* shells (PAS), sulfuric acid-treated *Pterospermum acerifolium* shells (SPAS), and phosphoric acid-treated *Pterospermum acerifolium* shells (PPAS) were inspected for the removal potential of Methylene blue and hexavalent chromium from aqueous solutions.

The morphological features of PAS, SPAS, and PPAS were evaluated through Environmental Scanning Electron Microscopy (E-SEM) analysis, using a Quanta 250 FEG. The chemical surface characterizations of the adsorbents were carried out by Fourier Transformed Infrared Spectroscopy (FT-IR). The adsorbent samples were prepared as pellets of potassium bromide, FT-IR measurements were performed using Spectrum Two model of Perkin Elmer FT-IR spectrophotometer, and the spectra was recorded at 4 cm^{-1} resolution in a range of 4000–400 cm^{-1}.

2.2. Chemicals

A stock solution of Methylene blue (MB) was prepared by dissolving an appropriate amount of MB dye in distilled water. Hexavalent chromium (Cr(VI)) stock solution was obtained by dissolving the requisite quantity of potassium dichromate ($K_2Cr_2O_7$) in distilled water. The experimental solutions of the required initial dye and metal concentrations were obtained by dilution of the stock solution with distilled water. Fresh dilutions were performed for the study on each adsorption process. The pH was adjusted to the desired value by adding HCl (0.1 N) and NaOH (0.1 N), before mixing the adsorbent to the solution. All the chemicals used in this study were of analytical grade and used without any further purification.

2.3. MB and Cr(VI) adsorption experiments

Batch adsorption experiments were carried out to explore the removal performance of PAS, SPAS, and PPAS toward MB and Cr(VI) in aqueous solutions. The parameters of the adsorption process such as adsorbent amount, initial solution pH, initial MB and Cr(VI) concentration, and temperature were investigated. The experimental studies were performed with known adsorbent dosage and desired concentration of MB and Cr(VI) at an optimum initial solution pH in 250 mL Erlenmeyer flasks, agitated on a thermostated shaking incubator at 120 rpm. The initial concentration of MB and Cr(VI) varied from 50 to 250 mg/L, the difference between the amount of adsorbate in the solution at equilibrium and initial concentration used in the determination of adsorption isotherm models. The experiments for evaluating adsorption kinetics were performed by contacting adsorbent with 50 mL of MB and Cr(VI) solution. At the predetermined time interval, samples were withdrawn to determine the adsorbate concentration using double beam UV–visible spectrophotometer (Systronics 2203). The concentration of MB was measured at a wavelength of 664 nm and Cr(VI) measurement done using a solution of 1, 5-diphenyl carbazide as the complexing agent in acid forms a pink color with Cr(VI), analyzed at 540 nm. The results presented are the mean values of the duplicated experiments.

The percentage of removal (%) and the amount of MB and Cr(VI) bound by the adsorbent (q_t) were calculated as follows:

$$\%\text{Removal} = \left[\frac{C_i - C_t}{C_i}\right] \times 100 \quad (1)$$

$$q_t = \left[\frac{C_i - C_t}{M}\right] \times V \quad (2)$$

where C_i and C_t are the initial and concentrations of adsorbates (mg/L) at time t, M is the amount of adsorbents (g), and V is the volume of the adsorbate solution (L).

2.4. Desorption and recyclability experiments

Desorption process refers to the reversed adsorption process, which involves removal of the from the adsorbent using a suitable desorption medium. The reusability of PAS, SPAS, and PPAS was evaluated by consecutive adsorption and desorption process. In this study, 0.1 N HCl and 0.1 N NaOH were used as the desorbing agent. The desorption study was performed similar to the adsorption experiments. The only difference involves the adsorbent loaded with MB and Cr(VI) as the result of adsorption process after drying was placed in the 50 mL of desorption solution. After desorption process, the adsorbent was washed thoroughly using distilled water to remove any residual desorbing solution in the adsorbent, further oven dried and reconditioned for the next cycle. The desorption experiments were carried out for the removal of MB and Cr(VI) using the three adsorbents PAS, SPAS, and PPAS and recyclability test conducted up to three cycles.

3. Adsorption theoretical background

3.1. Adsorption equilibrium

Adsorption isotherms offer main information on the adsorption process and describe the interaction of the adsorbate with the adsorbent. The relationship of equilibrium data through theoretical models is important in the design and functional aspects of the adsorption system. The adsorption isotherm correlations are vital in the assessment of adsorbent distribution on solid/liquid interface and in the estimation of the uptake capacity of adsorbent toward the pollutant removal. The thermodynamic assumptions of the adsorption isotherm models provide insight on the adsorption mechanism, adsorbent surface properties, and affinities toward the pollutant [23]. The results of the experimental adsorption data were modeled using the adsorption isotherm models such as Langmuir, Freundlich, Halsey, Jovanovic, Frumkin, and Kiselev.

3.1.1. Langmuir model

The Langmuir isotherm is the simplest and widely used model for describing the saturation type of adsorption isotherms. This model was initially used for the adsorption of gas onto activated carbon and later applied to the liquid system. In this model, the mass of solute adsorbed per unit adsorbent mass increases linearly by solute concentration increase at the lower surface coverage, and approaches asymptotic value under the condition of adsorption sites approach toward saturation. The Langmuir model assumes monolayer adsorption devoid of steric hindrance and no adsorbate transmigration in the surface plane, uniform adsorption energies onto the surface, and no interaction between adsorbed molecules [24]. The linear form of the Langmuir isotherm model is represented using the following equation:

$$\frac{C_e}{q_e} = \frac{1}{K_L Q_m} + \frac{C_e}{Q_m} \tag{3}$$

where q_e (mg/g) is the amount of MB and Cr(VI) adsorbed at equilibrium, C_e (mg/L) is the equilibrium concentration of the adsorbate, Q_m (mg/g) is the maximum adsorption capacity of the adsorbent, and K_L (L/mg) is the Langmuir constant, which is related to adsorption energy. The Langmuir isotherm model constant (K_L) is expressed in terms of a dimensionless constant (R_L), also referred to as the separation factor. The dimensionless separation factor finds its application in the prediction of adsorption process favorability. The constant of the Langmuir isotherm model and separation factor are related using the following equation:

$$R_L = \frac{1}{1 + K_L C_i} \tag{4}$$

3.1.2. Freundlich model

The Freundlich isotherm is another commonly used empirical model, describing the adsorption process type of non-ideal and reversible. This model is based on the assumption of multilayer adsorption mechanism and used to describe heterogeneous adsorbent surface without uniform distribution of the heat of adsorption [25]. The linear form of the Freundlich equation is given as:

$$\log q_e = \log K_F + \frac{1}{n_F} \log C_e \tag{5}$$

where K_F (mg/g) and n_F are Freundlich isotherm model constants related to the measure of adsorption capacity and adsorption intensity, respectively.

3.1.3. Halsey model

The Halsey isotherm model is suitable for explaining the multilayer adsorption, and fitting of this model to the adsorption equilibrium data is used to demonstrate the heteroporous nature of the adsorbent [26]. The linearized equation of the Halsey model is expressed as:

$$\ln q_e = \frac{1}{n_H} \ln K_H - \frac{1}{n_H} \ln \frac{1}{C_e} \tag{6}$$

where K_H is the Halsey isotherm model constant and n_H denotes the Halsey isotherm model exponent.

3.1.4. Jovanovic model

The Jovanovic isotherm model describes monolayer adsorption without lateral interactions as considered in the Langmuir isotherm assumption. The Jovanovic isotherm takes in the description of some possible mechanical contacts exhibited between adsorbing and desorbing molecules in a homogenous adsorbent surface [27]. The Jovanovic isotherm model is first applied for the gas adsorption, then for peptide and protein separation using ion-exchange adsorbents and copper biosorption [28]. The equation of this model is expressed as follows:

$$\ln q_e = \ln Q_0 - K_J C_e \tag{7}$$

where Q_0 (mg/g) represents the maximum adsorption capacity and K_J (L/mg) is the Jovanovic model constant.

3.1.5. Frumkin model

The Frumkin isotherm model describes the adsorption process on a homogenous surface and considers the interaction between the adsorbed species within the monolayer [29]. The Frumkin isotherm model is depicted as follows:

$$\ln\left[\left(\frac{\theta}{1-\theta}\right)\frac{1}{C_e}\right] = \ln K_{FK} + 2a_{FK}\theta \tag{8}$$

where K_{FK} represents the equilibrium constant, θ is the surface coverage, and a_{FK} is the interaction parameter of the Frumkin model. The value of a_{FK} is based on the interaction characteristic between the adsorbed molecules and can be either positive or negative. If $a_{FK} > 0$, it indicates attraction between adsorbate and repulsion in case of $a_{FK} < 0$.

3.1.6. Kiselev model

The Kiselev isotherm model predicts the adsorption characteristics in the localized monomolecular layer in the adsorbent [30]. The linear

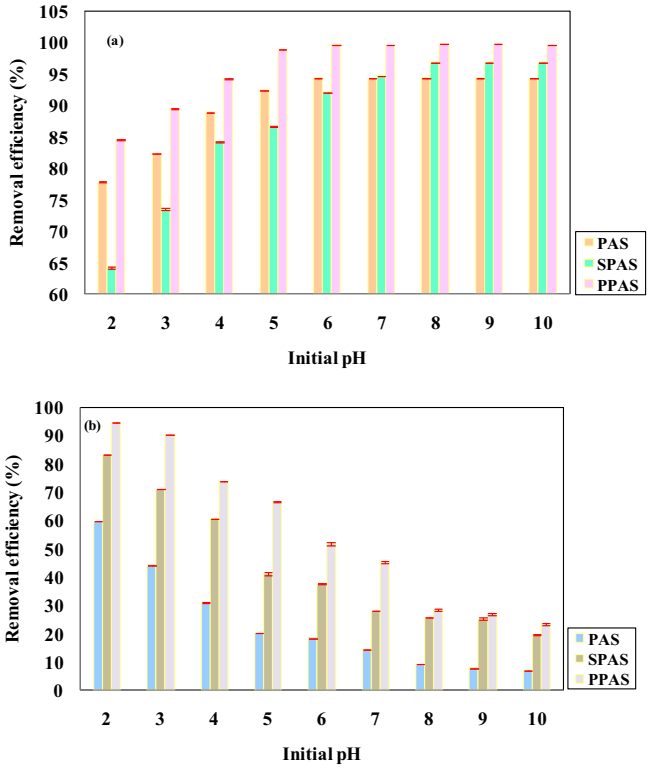

Fig. 1. Effect of initial pH on the percentage adsorption of (a) MB and (b) Cr(VI) using PAS, SPAS, and PPAS.

form of the Kiselev isotherm model is expressed using the following equation:

$$\frac{1}{C_e(1-\theta)} = \frac{K_{KL}}{\theta} + K_{KL}\,K_n \tag{9}$$

K_{KL} (L/mg) is the Kiselev equilibrium constant, θ denotes the surface coverage, and K_n represents the Kiselev constant of complex formation between the adsorbed molecules.

3.2. Adsorption kinetics

The adsorption kinetic models are useful in the rate determination of the removal process, and it is a significant factor in designing the adsorption system in addition to the adsorption capacity. Moreover, kinetics provides information on the removal mechanisms, which is based on the physico-chemical property of the adsorbent and mass transport process [31]. In order to understand the chemical interactions, mass transfer, and diffusion control in the adsorption process, kinetic models such as pseudo-first order, pseudo-second order, Elovich, and intra-particle diffusion were employed.

3.2.1. Pseudo-first order

The pseudo-first order equation or Lagergren equation [32] is based on the assumption that the adsorbate is assigned to an adsorption site on the adsorbent, expressed in terms of the rate of reaction. The pseudo-first order kinetic model relates the rate of adsorbate adsorption with time is directly proportional to the difference between the amount of adsorbate absorbed at time, t and the amount of adsorbate absorbed at equilibrium. The pseudo-first order kinetics model is defined as:

$$\frac{dq_t}{dt} = k_1(q_e - q_t) \tag{10}$$

The expression of the pseudo-first order kinetic model given as follows:

$$\log(q_e - q_t) = \log q_e - \frac{k_1}{2.303}t \tag{11}$$

where q_t (mg/g) and q_e (mg/g) are the amount of adsorbate uptake by the adsorbent at time t and equilibrium, respectively. k_1 (1/min) denotes the pseudo-first order kinetic model rate constant.

3.2.2. Pseudo-second order

Blanchard, et al. first proposed the pseudo-second-order kinetic model in 1980 [33]. In the later years, Ho and MacKay [34] modified this model and applied for the removal of pollutant using different adsorbents, which is widely in use by many researchers in the adsorption studies of wastewater pollutants removal. The correlation of the pseudo-second order model states that the adsorption rate of the adsorbate uptake is directly proportional to the square of the difference between the amount of adsorbate absorbed at time, t and the amount of adsorbate absorbed at equilibrium. The pseudo-second order kinetics model is defined as:

$$\frac{dq_t}{dt} = k_2(q_e - q_t)^2 \tag{12}$$

$$\frac{t}{q_t} = \frac{1}{k_2 q_e^2} + \frac{t}{q_e} \tag{13}$$

where q_t (mg/g) and q_e (mg/g) are the uptake amount of the adsorbate by the adsorbent at time t and equilibrium, respectively. k_2 (g/mg min)

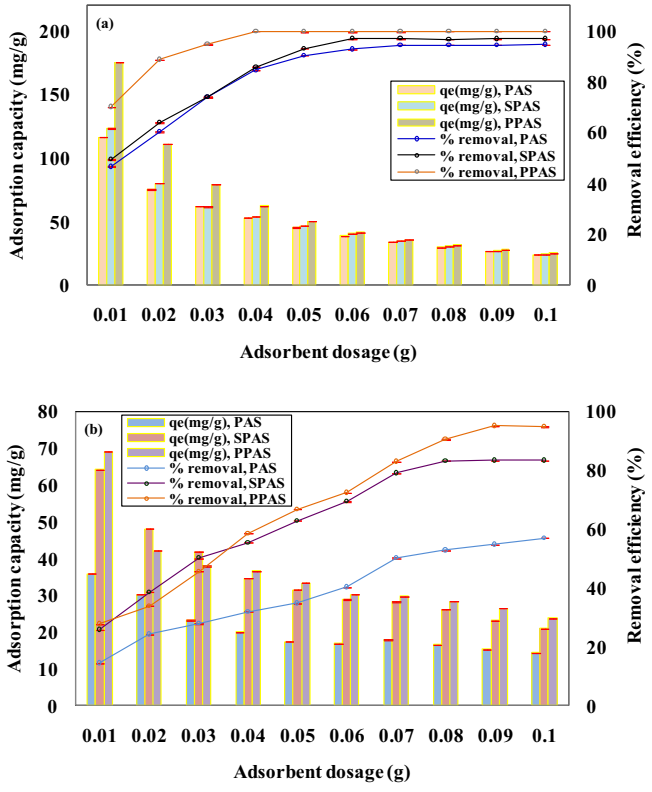

Fig. 2. Effect of PAS, SPAS, and PPAS dosage on the adsorption capacity and removal efficiency toward (a) MB and (b) Cr(VI).

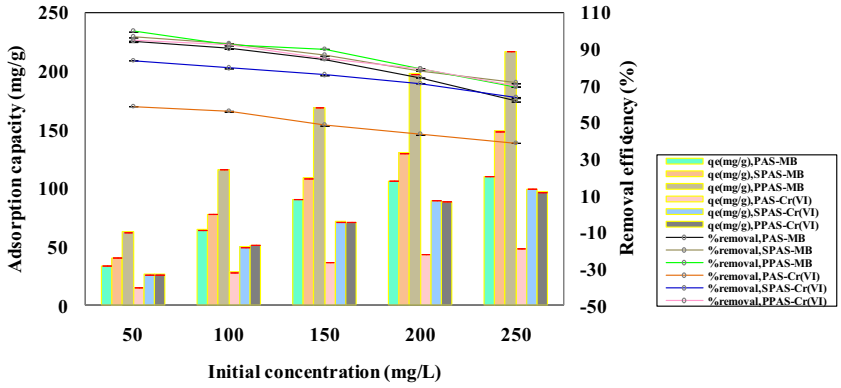

Fig. 3. Effect of initial MB and initial Cr(VI) concentration on adsorption capacity and removal efficiency using PAS, SPAS, and PPAS.

represents the rate constant of the pseudo-second order kinetic model rate constant.

3.2.3. Elovich

The Elovich kinetic model [35] adequately describes some chemisorption processes and covers a wide range of slow removal rates by the adsorbent. This model is valid for adsorption systems with a heterogeneous surface. The Elovich model considers the assumption that the heterogeneous adsorption sites of the adsorbent display different activation energies during the removal process. The Elovich kinetic model is given as follows:

$$q_t = \frac{1}{\beta}\ln(\alpha\beta) + \frac{1}{\beta}\ln t \tag{14}$$

where α (mg/g min) is the initial rate of adsorption and β (g/mg) is the constant of Elovich kinetic model.

Table 1
Thermodynamic parameters for adsorption of MB and Cr(VI) onto PAS, SPAS, and PPAS.

MB adsorption										
C_i (mg/L)	T (K)	PAS			SPAS			PPAS		
		$\Delta G°$ (kJ/mol)	$\Delta H°$ (kJ/mol)	$\Delta S°$ (J/mol K)	$\Delta G°$ (kJ/mol)	$\Delta H°$ (kJ/mol)	$\Delta S°$ (J/mol K)	$\Delta G°$ (kJ/mol)	$\Delta H°$ (kJ/mol)	$\Delta S°$ (J/mol K)
50	303	−6.18	45.46	169.52	−8.06	−57.86	−165.19	−16.11	−139.76	−411.79
	313	−7.07			−5.56			−8.41		
	323	−9.60			−4.79			−8.01		
100	303	−4.75	20.10	81.95	−6.04	−56.60	−168.10	−6.92	−50.58	−144.58
	313	−5.51			−3.16			−4.97		
	323	−6.39			−2.73			−4.05		
150	303	−3.42	5.99	31.06	−4.24	−48.97	−148.40	−6.11	−63.99	−191.80
	313	−3.75			−2.02			−3.40		
	323	−4.04			−1.30			−2.30		
200	303	−1.81	9.24	36.33	−2.73	−31.39	−95.02	−3.91	−48.79	−148.82
	313	−2.05			−1.33			−1.68		
	323	−2.54			−0.85			−0.97		
250	303	−0.34	9.39	32.20	−1.84	−24.61	−75.82	−2.63	−35.72	−109.66
	313	−0.72			−0.43			−1.10		
	323	−0.98			−0.35			−0.45		
Cr(VI) Adsorption										
C_i (mg/L)	T (K)	PAS			SPAS			PPAS		
		$\Delta G°$ (kJ/mol)	$\Delta H°$ (kJ/mol)	$\Delta S°$ (J/mol K)	$\Delta G°$ (kJ/mol)	$\Delta H°$ (kJ/mol)	$\Delta S°$ (J/mol K)	$\Delta G°$ (kJ/mol)	$\Delta H°$ (kJ/mol)	$\Delta S°$ (J/mol K)
50	303	0.86	12.40	38.34	−2.92	26.66	97.52	−5.79	17.48	77.00
	313	0.25			−3.80			−6.76		
	323	0.10			−4.88			−7.32		
100	303	1.14	12.40	37.25	−2.24	14.66	55.81	−4.77	18.53	76.85
	313	0.70			−2.81			−5.50		
	323	0.40			−3.35			−6.30		
150	303	1.91	16.22	46.89	−1.69	26.66	93.36	−2.88	24.03	88.71
	313	1.76			−2.480			−3.71		
	323	0.96			−3.56			−4.66		
200	303	2.42	14.30	39.14	−1.11	26.65	91.28	−1.91	20.49	73.96
	313	2.09			−1.74			−2.65		
	323	1.63			−2.94			−3.39		
250	303	2.94	15.58	41.62	−0.21	21.55	71.94	−0.59	17.39	59.25
	313	2.61			−1.06			−1.08		
	323	2.10			−1.64			−1.78		

3.2.4. Intra-particle diffusion

According to intra-particle diffusion model developed by Weber and Morris, the uptake of the adsorbate by the adsorbent varies almost proportionally with the square root of contact time *t*, rather than varying in direct proportion with the contact time. The assumption of intra-particle diffusion [36] is based on the transport of the adsorbate through the internal porous structure of the adsorbent and diffusion in the solid, illustrates the homogeneous porous structure of the adsorbent and intra-particle diffusion as the rate-limiting step of an adsorption system.

$$q_t = k_{id}\sqrt{t} + I \tag{15}$$

where k_{id} denotes the constant of intra-particle diffusion model (mg/g $min^{0.5}$) and *I* indicates the boundary layer thickness (mg/g).

4. Results and discussion

4.1. Influence of initial solution pH

The initial pH of the adsorption medium is one of the most influential parameters in the process of adsorption due to factors such as protonation or deprotonation of the adsorbent active sites, interactions between the adsorbate, and the degree of ionization of adsorbate molecules in the aqueous solution. In the present study, the adsorption experiments were performed in the initial solution pH range from 2.0 to 10.0, and the respective removal efficiency of PAS, SPAS, and PPAS toward MB and Cr(VI) are shown in Fig. 1a and b. The effect of solution pH on the adsorption of MB and Cr(VI) was studied with an initial concentration of 50 mg/L. The results of the MB adsorption using PAS, SPAS, and PPAS showed that the percentage removal of MB increased with increase in the initial solution pH. The maximum removal of MB using PAS (94.37%), SPAS (96.79%), and PPAS (99.66%) was observed at the initial pH of 6.0, 8.0, and 6.0, respectively. The lesser removal efficiency of the adsorbents at lesser pH range was due to the occurrence of more amounts of free protons in the aqueous solution and consequent to the competitive effect of binding with MB for the adsorption sites on the adsorbents [37]. At the higher initial solution pH, the enhanced removal efficiency of the MB may be attributed to the increase in hydroxide ions on the adsorbent's surface, which causes strong electrostatic attraction between the cationic MB molecule and the negatively charged adsorbent surface. Therefore, the initial solution pH of 6.0, 8.0, and 6.0 was selected as the optimal pH for MB adsorption using PAS, SPAS, and PPAS, respectively.

The role of the initial pH was examined for the adsorption of Cr(VI) using PAS, SPAS, and PPAS, and the results of the removal performance were presented in Fig. 1b. The percentage removal of Cr(VI) declined from 59.71% to 6.98% (PAS), 83.26% to 19.58% (SPAS), and 94.62% to 23.34% (PPAS), respectively, for the increase of initial pH from 2.0 to 10.0. Maximum removal efficiency of Cr(VI) ions by the three adsorbents were attained at the initial pH 2.0. The results revealed that pH depended the adsorption process on the basis of ionic forms of chromium ions in solutions and surface properties changes of the adsorbent. At the acidic pH range of the aqueous solution, Cr(VI) ions occur in the forms of hydrogen chromate ($HCrO_4^-$) and chromate (CrO_4^{2-}). At the higher acidic pH value of 2.0, hydrogen chromate is the predominant form of Cr(VI) ions and shows more affinity toward the protonated adsorbent surface, causes electrostatic attraction, and favors the adsorption of negatively charged hydrogen chromate ions from the aqueous solution [38]. With further increase in the initial pH from 2.0 to 10.0, there observed a decrease in the removal efficiency of Cr(VI) by the adsorbents. The results are due to the drop of protons in the aqueous solution with increasing pH, increase in the negative charge density at the adsorbent surface and resultant in the competitive or repulsive effect between the increased hydroxide ions and hydrogen chromate ions for adsorbent binding. Based on the results of removal efficiency of Cr

Table 2
Adsorption isotherm model parameters and coefficient of determination for removal of MB and Cr(VI) using PAS, SPAS, and PPAS.

Isotherms	MB adsorption			Cr(VI) adsorption		
	PAS	SPAS	PPAS	PAS	SPAS	PPAS
Langmuir						
Q_m (mg/g)	125.00	166.66	250.00	76.92	142.85	111.11
K_L (L/mg)	0.129	0.130	0.222	0.012	0.027	0.105
R^2	0.999	0.993	0.992	0.994	0.996	0.997
Freundlich						
K_F (mg/g)	26.60	36.39	92.89	2.73	8.51	20.37
n_F	2.923	2.932	5.208	1.715	1.763	2.610
R^2	0.926	0.982	0.964	0.967	0.975	0.956
Halsey						
K_H	6.79×10^{-5}	2.63×10^{-5}	5.63×10^{-11}	0.17	0.02	3.80×10^{-4}
n_H	−2.923	−2.935	−5.208	−1.715	−1.763	−2.610
R^2	0.926	0.982	0.964	0.967	0.975	0.956
Jovanovic						
Q_0 (mg/g)	51.98	59.38	97.02	16.36	32.72	39.29
K_J (L/mg)	−0.009	−0.015	−0.012	−0.008	−0.014	−0.014
R^2	0.570	0.701	0.617	0.810	0.768	0.664
Frumkin						
K_{FK}	3.58×10^{-7}	1.51×10^{-9}	4.54×10^{-13}	2.30×10^{-5}	3.28×10^{-7}	1.15×10^{-8}
a_{FK}	8.33	11.51	16.78	6.59	8.42	10.27
R^2	0.919	0.922	0.728	0.969	0.950	0.930
Kiselev						
K_{KL} (L/mg)	9.873	44.37	5.488	0.246	2.272	17.54
K_n	−0.672	−0.761	−0.718	−3.90	−0.662	−0.724
R^2	0.356	0.406	0.632	0.671	0.566	0.440

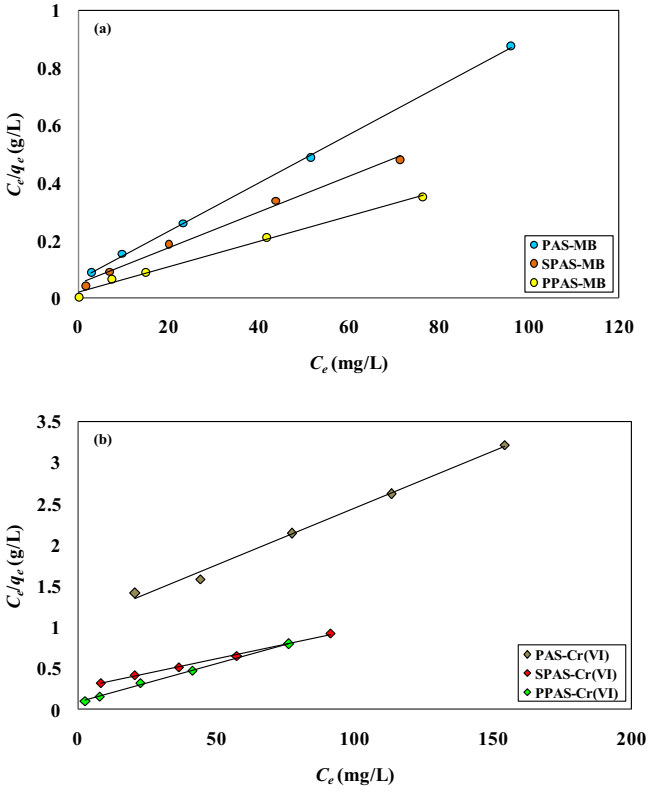

Fig. 4. Linear fitting of Langmuir isotherm for the adsorption of (a) MB and (b) Cr(VI) using PAS, SPAS, and PPAS.

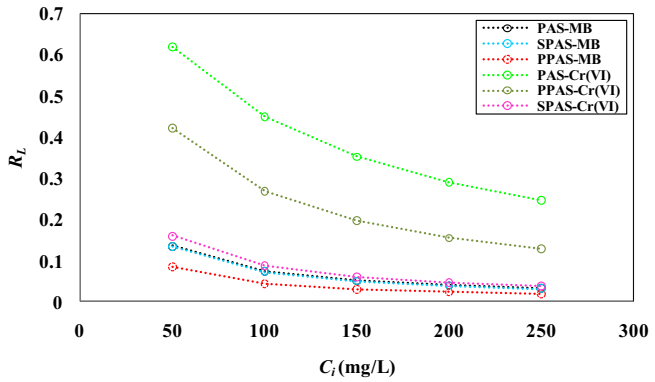

Fig. 5. Plots of dimensionless separation factor.

(VI) removal, the optimum pH value of 2.0 was considered for the rest of the adsorption study.

4.2. Influence of adsorbent dosage

Adsorbent dosage is a vital parameter in the removal assessment of MB and Cr(VI) from the aqueous solution as it ascertains equilibrium between the adsorbate and adsorbent in the adsorption system and adsorption capacity of the adsorbent. In order to illustrate the probability of adsorption of MB and Cr(VI) by an adsorbent at the optimal pH and fixed initial adsorbate concentration, the dosage of PAS, SPAS, and PPAS were varied from 0.01 g to 0.1 g. The effect of adsorbent dosage on the uptake capacity and percentage removal of MB and Cr(VI) at equilibrium condition is illustrated in Fig. 2a and b. The removal efficiency for MB increased with the adsorbent dosage increase (Fig. 2a) to a different extent based on the adsorbent, 46.50% to 94.25% (PAS), 49.29% to 96.79% (SPAS), and 69.91% to 99.62% (PPAS), respectively. The maximum MB adsorption efficiency was observed at the dosage of (0.07 g) PAS, (0.06 g) SPA, and (0.04 g) PPAS, beyond these adsorbent dosage the removal efficiency of the adsorbent remains almost the same. The results are due to the more number of binding sites on the adsorbents by increase of the adsorbent dosage. Nevertheless, a further increase from the optimal adsorbent dosage did not show significant changes, because adsorption reaches saturation [39]. The adsorption efficiency for the removal of Cr(VI) increases from 14.33% to 56.94% (PAS), 25.66% to 83.26% (SPAS), and 27.64% to 95.12% (PPAS), with the increase of adsorbent dosage. The higher removal efficiency of Cr(VI) was found at the dosage of (0.1 g) PAS, (0.08 g) SPA, and (0.09 g) PPAS, respectively.

The results of the adsorbent dosage, i.e., percentage removal and adsorption capacity presented opposite trend with the increase of the adsorbent dosage. At the low adsorbent dosage of 0.01 g, higher adsorption capacity of 116.25 mg/g (PAS), 123.22 mg/g (SPAS), and 174.79 mg/g (PPAS) for MB removal and adsorption capacity of 14.23 mg/g (PAS), 83.26 mg/g (SPAS), and 95.12 mg/g (PPAS) for Cr (VI) removal, respectively, was observed. The uptake capacity toward MB and Cr(VI) removal was higher at the adsorbent dosage of 0.01 g

Table 3
Adsorption kinetic model parameters and coefficient of determination for the removal of MB and Cr(VI) using PAS, SPAS, and PPAS.

	MB	Pseudo-first order			Pseudo-second order			Elovich			Intra-particle diffusion		
	C_i (mg/L)	k_1 (1/min)	q_e(cal) (mg/g)	R^2	k_2 (g/mg min)	q_e(cal) (mg/g)	R^2	α (mg/g min)	β (g/mg)	R^2	k_{id} (mg/g $min^{0.5}$)	I (mg/g)	R^2
MB	PAS												
	50	0.0391	14.22	0.837	0.0068	35.71	0.999	15.90×10^4	0.4791	0.901	0.624	26.89	0.929
Adsorption	100	0.0391	32.88	0.914	0.0025	71.42	0.999	2233.58	0.1648	0.974	1.736	46.38	0.919
	150	0.0368	48.52	0.897	0.0014	100.00	0.998	1950.54	0.1128	0.954	2.612	62.64	0.955
	200	0.0368	60.95	0.924	0.0010	125.00	0.999	761.15	0.0841	0.941	3.462	69.58	0.921
	250	0.0414	74.64	0.949	0.0010	125.00	0.998	377.41	0.0736	0.926	3.891	68.62	0.877
	SPAS												
	50	0.0391	12.10	0.866	0.0104	41.66	0.999	18.87×10^6	0.5173	0.979	0.573	34.54	0.893
	100	0.0345	23.82	0.829	0.0040	83.33	0.999	57.83×10^6	0.2779	0.965	1.064	65.69	0.973
	150	0.0368	51.88	0.932	0.0014	125.00	0.999	5687.13	0.1029	0.963	2.803	78.61	0.924
	200	0.0275	49.43	0.836	0.0014	142.85	0.999	13.30×10^4	0.1125	0.943	2.663	99.96	0.977
	250	0.0345	87.09	0.929	0.0007	166.66	0.998	1202.62	0.0617	0.973	4.741	97.11	0.961
	PPAS												
	50	0.0713	27.54	0.917	0.0097	66.66	0.999	11.58×10^7	0.3539	0.876	0.759	54.80	0.730
	100	0.0575	69.82	0.944	0.0020	125.00	0.999	9822.49	0.0993	0.908	2.790	87.53	0.802
	150	0.0460	112.20	0.899	0.0006	200.00	0.998	1192.81	0.0524	0.930	5.484	111.80	0.885
	200	0.0529	118.03	0.935	0.0008	250.00	0.999	6240.87	00524	0.915	5.242	145.00	0.798
	250	0.0598	98.40	0.895	0.0020	250.00	0.999	50.87×10^5	0.0808	0.879	3.318	183.00	0.729
	Cr(VI)												
Cr(VI)	C_i (mg/L)	PAS											
Adsorption	50	0.0276	11.85	0.884	0.0032	16.66	0.985	5.10	0.3868	0.917	0.787	5.88	0.980
	100	0.0345	23.65	0.909	0.0021	31.25	0.995	11.94	0.2076	0.961	1.423	12.39	0.968
	150	0.0230	21.72	0.911	0.0015	41.66	0.984	29.49	0.1798	0.893	1.078	18.04	0.972
	200	0.0230	31.69	0.913	0.0008	52.63	0.975	13.12	0.1252	0.892	2.462	16.49	0.977
	250	0.0184	31.11	0.884	0.0008	55.55	0.976	18.38	0.1240	0.882	2.490	19.24	0.971
	SPAS												
	50	0.0460	8.317	0.983	0.0175	27.02	1.00	15.57×10^5	0.7092	0.922	0.385	22.21	0.792
	100	0.0299	25.94	0.912	0.0024	52.63	0.998	432.79	0.1878	0.977	1.569	32.30	0.979
	150	0.0253	40.17	0.917	0.0012	76.92	0.996	177.43	0.1127	0.960	2.647	41.17	0.985
	200	0.0345	74.47	0.864	0.0006	100.00	0.991	69.48	0.0748	0.880	4.080	43.29	0.946
	250	0.0276	75.68	0.912	0.0005	111.11	0.989	48.71	0.0618	0.912	4.915	43.70	0.971
	PPAS												
	50	0.0391	13.09	0.888	0.0073	27.77	0.999	4788.71	0.4770	0.951	0.614	19.74	0.941
	100	0.0299	25.94	0.845	0.0025	55.55	0.997	1308.52	0.2058	0.909	1.461	35.09	0.947
	150	0.0299	43.65	0.866	0.0012	76.92	0.994	162.17	0.1106	0.898	2.733	40.69	0.947
	200	0.0253	54.70	0.898	0.0008	100.00	0.995	83.19	0.0764	0.963	3.874	45.94	0.973
	250	0.0345	63.38	0.937	0.0008	111.11	0.997	162.31	0.0760	0.954	3.845	55.26	0.940

for all the three adsorbents and the further increase of adsorbent dosage showed decreased effect. The results are likely due to the available free adsorption sites on the adsorbents; the lower adsorbate equilibrium concentration at high adsorbent concentrations, and leftover unsaturated adsorption sites [40]. The optimal dosage value for the adsorption of MB and Cr(VI) was selected from the results of percentage removal efficiency.

4.3. Influence of MB and Cr(VI) initial concentration

The initial concentration of the adsorbate in the aqueous solution acts as the driving force in order to maintain the balance of resistance due to mass transfer between the adsorbate and adsorbent molecules. The initial concentrations of MB and Cr(VI) were studied in the range of 50–250 mg/L at the optimal adsorbent dosage and initial pH for the assessment of initial adsorbate concentration effect on removal performance by the adsorbents. Fig. 3 presents the variation of uptake capacity and percentage removal of MB and Cr(VI) by PAS, SPAS, and PPAS. The results represented that the adsorption capacity toward MB removal increased from 33.64 mg/g to 109.89 mg/g (PAS), 40.29 mg/g to 148.69 mg/g (SPAS), and 62.36 mg/g to 216.92 mg/g (PPAS). For the Cr(VI) removal, the adsorption capacity increased from 14.66 mg/g to 47.98 mg/g (PAS), 26.13 mg/g to 99.17 mg/g (SPAS), and 26.30 mg/g to 96.53 mg/g (PPAS), respectively. The increase of initial adsorbate concentration from 50 mg/L to 250 mg/L showed raise of the adsorption capacity for the removal of MB and Cr(VI). The results are due to higher utilization of adsorbent active sites, competing effect by more adsorbate molecules for the adsorbent binding sites, and increase in the driving force of the concentration gradient [41]. Fig. 3 shows the decrease in the adsorbate percentage removal of MB and Cr(VI) with the increase of initial adsorbate concentration from 50 mg/L to 250 mg/L. The adsorption efficiency decreased from 94.20% to 61.54% (PAS), 96.70% to 71.37% (SPAS), and 99.79% to 69.41% (PPAS) for MB removal. In case of Cr(VI) adsorption, the removal efficiency decreased from 58.67% to 38.38% (PAS), 83.63% to 63.47% (SPAS), and 99.71% to 69.50% (PPAS), respectively. The removal efficiency of PAS, SPAS, and PPAS for the adsorption of MB and Cr(VI) was found higher at the lower concentration of 50 mg/L, and the further increase of initial concentration showed decreased removal efficiency due to the rapid saturation of adsorbate binding sites on the adsorbent surface. Therefore, 50 mg/L was selected as the optimum initial concentration of MB and Cr(VI) for the adsorption experiments.

4.4. Influence of temperature and thermodynamic study of adsorption

The effect of temperature on the adsorption of MB and Cr(VI) on PAS, SPAS, and PPAS were studied in the temperature range of 303–323 K for 50–250 mg/L initial adsorbate concentration. For the adsorption of MB by PAS, the removal performance found higher at 323 K, whereas for SPAS and PPAS observed decreased effect for the increase in temperature from 303 K to 323 K. In case of the adsorption of Cr(VI) using PAS, SPAS and PPAS, the removal performance for the initial Cr(VI) concentration of 50–250 mg/L was found increased for the temperature increase from 303 K to 323 K (Figure not shown).

The thermodynamic parameters, including Gibbs free energy change (ΔG°), enthalpy change (ΔH°), and entropy change (ΔS°) were calculated according to the following equations:

$$\Delta G^\circ = -RT \ \ln k_c \tag{16}$$

$$\ln k_c = \frac{-\Delta H^\circ}{RT} + \frac{\Delta S^\circ}{R} \tag{17}$$

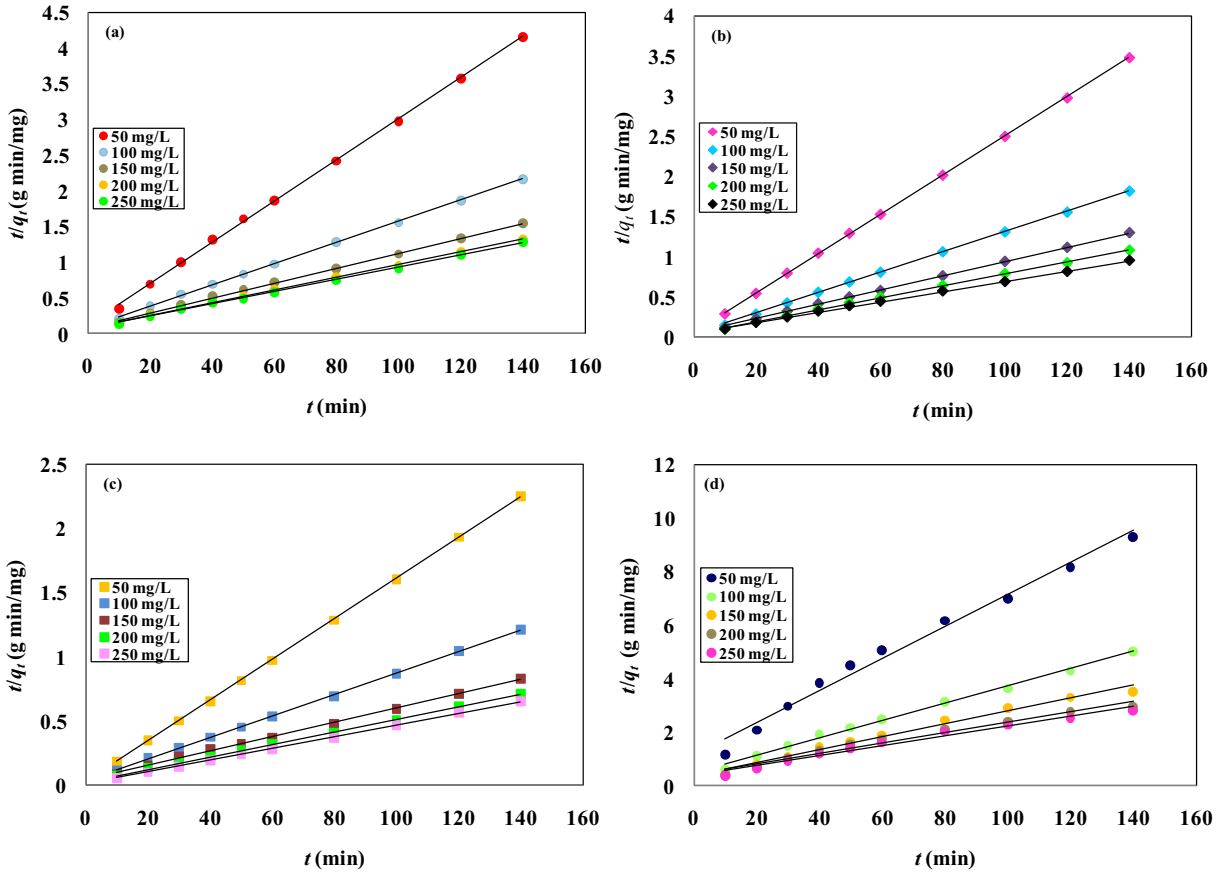

Fig. 6. Pseudo-second order adsorption kinetic model for MB adsorption using (a) PAS, (b) SPAS, and (c) PPAS and Cr(VI) adsorption using (d) PAS, (e) SPAS, and (f) PPAS.

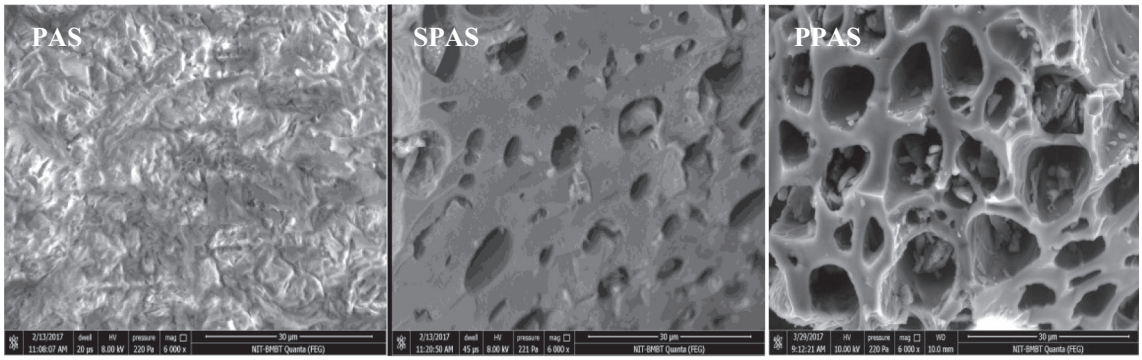

Fig. 7. E-SEM images of the unmodified and acids-modified *Pterospermum acerifolium* shells (magnification 6000×).

where R represents universal gas constant (8.314 J/mol K), T is temperature (K), and k_c indicate the distribution coefficient given by $k_c = {}^{q_e}/_{C_e}$.

The values of $\Delta G°$ are obtained from Eq. (16), while the values of $\Delta H°$ and $\Delta S°$ are determined from the slope and intercept of linear Van't Hoff plots (Eq. (17)) of ln k_c versus $1/T$. The calculated thermodynamic values of $\Delta G°$, $\Delta H°$, and $\Delta S°$ for the adsorption of MB and Cr(VI) using PAS, SPAS, and PPAS are given in Table 1. The negative values of $\Delta G°$ for the adsorption of MB by means of PAS, SPAS, and PPAS revealed that the adsorption process was spontaneous in nature and thermodynamically favorable. The positive values of $\Delta H°$ confirmed the endothermic nature of MB adsorption onto PAS, and $\Delta S°$ positive values indicated the increase in adsorption disorder. Whereas negative values of $\Delta H°$ and $\Delta S°$ observed in the adsorption of MB by SPAS and PPAS revealed the adsorption process as exothermic and not entropy driven. Positive values of $\Delta H°$ for the PAS, SPAS, and PPAS noted toward Cr(VI) removal, represented the endothermic nature of the adsorption process. Moreover, the values of $\Delta S°$ were also found as positive, which showed the PAS, SPAS, and PPAS affinity toward the Cr(VI) and also suggested the increased randomness at the interface region of the adsorbent and aqueous solution [42]. Negative values of $\Delta G°$ for the adsorption of Cr(VI) by SPAS and PPAS demonstrated the favorable adsorption process, except PAS showed positive value for Cr(VI) adsorption and represented the non-spontaneous nature of the adsorption process.

4.5. Adsorption isotherms

The adsorption equilibrium data were fitted with the isotherm models of Langmuir, Freundlich, Halsey, Jovanovic, Frumkin, and Kiselev. The corresponding values of estimated isotherm parameters along with the coefficient of determination (R^2) are summarized in Table 2. The Langmuir isotherm found better fitted for MB and Cr(VI) adsorption by PAS, SPAS, and PPAS adsorbents and the results are presented in Fig. 4a and b. The Langmuir isotherm model fitted well with the experimental adsorption data with a higher coefficient of determination values for MB adsorption, 0.999 (PAS), 0.993 (SPAS), and 0.992 (PPAS) and for Cr(VI) adsorption are 0.994 (PAS), 0.996 (SPAS), and 0.997 (PPAS), respectively. The better fit of the Langmuir model attests the strong monolayer interaction between MB and Cr(VI) molecules and the surface of PAS, SPAS, and PPAS. The Langmuir maximum adsorption capacity was determined as 125 mg/g (PAS), 166.66 mg/g (SPAS), and 250 mg/g (PPAS) for MB adsorption, and 76.92 mg/g (PAS), 142.85 mg/g (SPAS), and 111.11 mg/g (PPAS) for Cr(VI) adsorption. These results point out that monolayer adsorption capacity increases with pretreatment. Comparatively, PPAS and SPAS demonstrated higher adsorption capacity toward the removal of MB and Cr (VI). The values of dimensionless separation factor determined using the Langmuir isotherm constant and initial adsorbate concentrations are found in the range of 0–1, indicated favorable adsorption process

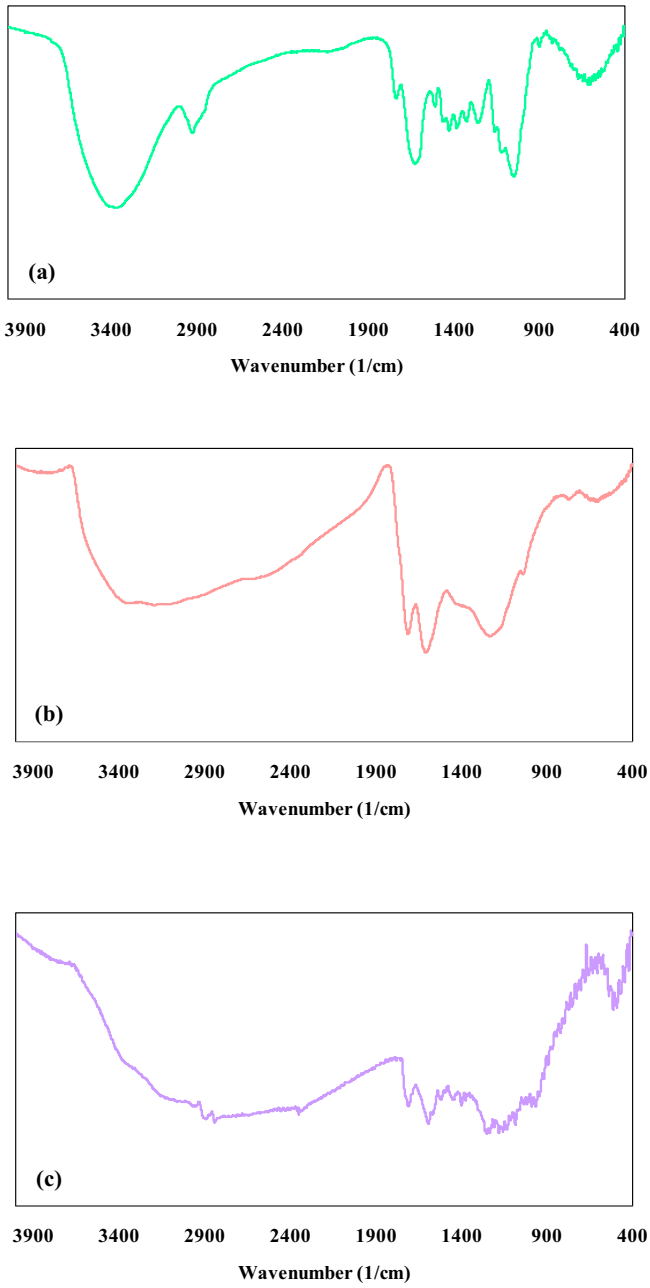

Fig. 8. FT-IR spectrum of (a) PAS, (b) SPAS, and (c) PPAS.

of both MB and Cr(VI) by the adsorbents. The variations of dimensionless separation factor as a function of initial adsorbate concentrations are illustrated in Fig. 5. The higher adsorption capacities and lower dimensionless separation factor values showed that PAS, SPAS, and PPAS as potential adsorbents for MB and Cr(VI).

The R^2 values for the Freundlich and Halsey isotherm fits are 0.926 (PAS), 0.982 (SPAS), and 0.964 (PPAS) for MB adsorption and 0.967 (PAS), 0.975 (SPAS), and 0.956 (PPAS) for Cr(VI) adsorption. The Freundlich and Halsey isotherm models better fitted the equilibrium data next to the Langmuir isotherm model. The calculated values of the Freundlich isotherm model constant, n_F, were in the range of 1.0–6.0 represented the adsorption phenomenon occurred more favorably by the PAS, SPAS, and PPAS, respectively [43]. The maximum adsorption capacity predicted using the Jovanovic isotherm model for MB adsorption are 51.98 mg/g (PAS), 59.38 mg/g (SPAS), and 97.02 mg/g (PPAS) and for Cr(VI) adsorption are 16.36 mg/g (PAS), 32.72 mg/g (SPAS), and 39.29 mg/g (PPAS). These values were found lower than the adsorption capacities found according to the Langmuir model. Moreover, R^2 values of Jovanovic were found lower than the values of Langmuir, Freundlich, and Halsey isotherm models, represented the less applicability of this model. The Frumkin isotherm model better described the adsorption process than the Jovanovic isotherm. The values of interaction parameter of the Frumkin model (a_{FK}) were found >0, which revealed that attraction existed between adsorbate molecules. Comparatively, poor agreement was found for the Kiselev isotherm model (Table 2) fit with the experimental adsorption data and this indicated the least fit of Kiselev isotherm model.

4.6. Adsorption kinetics

To examine the rate-controlling step and mechanisms involved in the adsorption of MB and Cr(VI) using adsorbents, the adsorption kinetic models such as pseudo-first order, pseudo-second order, Elovich, and intra-particle diffusion were applied to the experimental data. The values of the kinetic model parameters obtained from the linear plots of Eqs. (11), (13), (14), and (15) together with their respective coefficient of determination (R^2) are illustrated in Table 3. The low R^2 values of the pseudo-first order kinetic model provided moderate correlation for the adsorption of MB and Cr(VI) using PAS, SPAS, and PPAS, which represented the less applicability of the pseudo-first order kinetic model. The pseudo-second order kinetic model for the removal of MB and Cr(VI) by the three adsorbents indicated highest R^2 value of >0.99, except Cr(VI) adsorption by PAS showed R^2 value of >0.97. The plots of the best fit of pseudo-second order kinetic model with the experimental data of the adsorption study carried out are depicted in Fig. 6 (a–f). The kinetic model result analysis confirmed that the pseudo-second order kinetic model best described the experimental adsorption data for MB and Cr(VI) removal by the three adsorbents. The best fit of

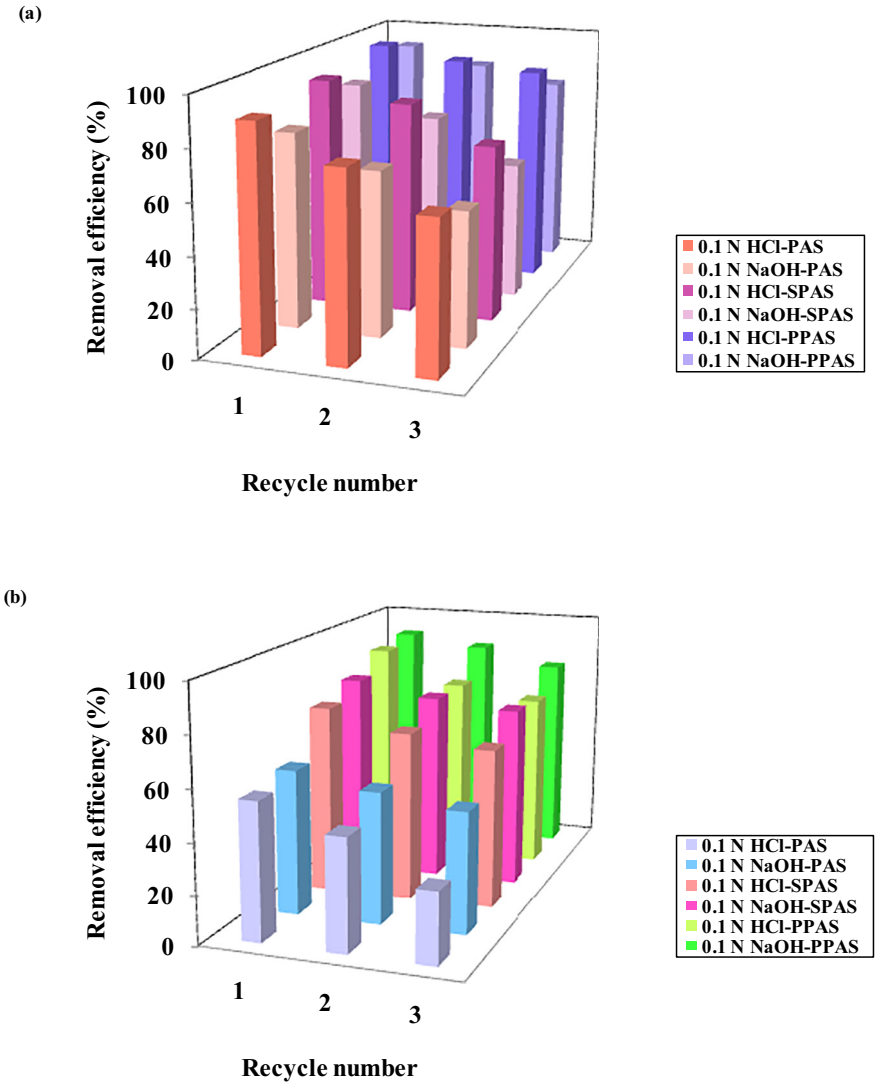

Fig. 9. Percentage removal of (a) MB and (b) Cr(VI) using PAS, SPAS, and PPAS in three cycles.

the pseudo-second order kinetic model confirmed that the rate-limiting step of the adsorption process governed by chemisorption. The adsorption data of MB and Cr(VI) removal was better described by pseudo-second order kinetic model than the pseudo-first order kinetic model, because pseudo-second order kinetic model was applicable for the entire contact time of the adsorption process, while pseudo-first order kinetic model was appropriate only in the initial contact time [44,45]. In case of the Elovich kinetic model, the R^2 values were found <0.98, which indicated that experimental adsorption data did not fit well with this model. The plots of an intra-particle diffusion model for each initial concentration of MB and Cr(VI) presented the lines without passing through the origin (Figure not shown). This result demonstrated that intra-particle diffusion model was not only the rate-determining step, additional adsorption processes and external mass transfer were related to boundary layer control for adsorbate adsorption. The observation of R^2 values (Table 3) suggested that the intra-particle diffusion kinetic model fit was not in good agreement with the experimental data [46].

4.7. Surface characteristics of PAS, SPAS, and PPAS

The E-SEM analysis is helpful to understand the morphological changes of *Pterospermum acerifolium* shells subjected to the sulfuric acid and phosphoric acid treatments. The photographs of the E-SEM analysis of PAS, SPAS, and PPAS are indicated in Fig. 7. The E-SEM micrographs of PAS show dense, rough, and heterogeneous surface without pores. The SPAS surface presents enhanced porosity; the occurrence of pores with different shapes and sizes illustrated SPAS texture was distributed with micropores and macropores. The sulfuric acid activation was mainly responsible for the porosity development in the precursor of *Pterospermum acerifolium* shells. The E-SEM image of PPAS represented similar structure of honeycomb pattern. The external surface of the PPAS showed full of cavities, adjacent cavities with organized macropores network, and the macropores are distributed with fine cylindrical structure bordered with perfect layers of carbon. The micrographs of SPAS and PPAS revealed that the porous structure developments are the resultant of precursor matrix decomposition by the sulfuric acid, phosphoric acids impregnation, and tars evaporation during the pretreatment process. The yields of SPAS and PPAS were determined as 32.19% and 39.24%.

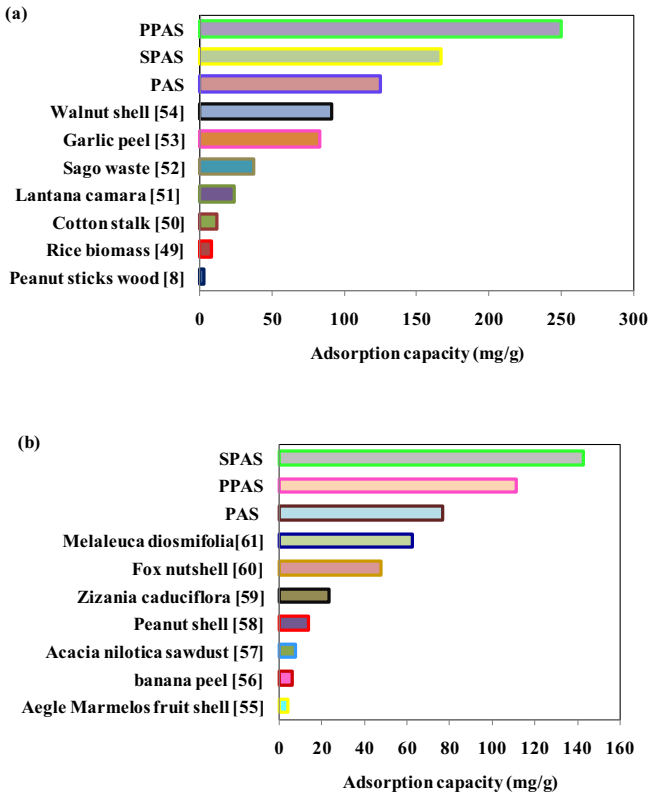

Fig. 10. Comparison of adsorption capacities of various adsorbents with PAS, SPAS, and PPAS for (a) MB [8,49–54] and (b) Cr(VI) removal [55–61].

4.8. Surface functional groups of the adsorbents

The chemical structures of the adsorbents are comprehended through characterization of functional groups on the adsorbents. The explanations regarding spectra shift, peak decrease, and disappearance are used to analyze the influence of acids pretreatment on the precursor used. The distribution of functional groups on the adsorbent surface was studied by means of FT-IR analysis. The results of FT-IR spectra patterns of PAS, SPAS, and PPAS were shown in Fig. 8(a–c). The FT-IR spectra results displayed a large number of absorption peaks in all the three adsorbents and demonstrated the complex nature of the adsorbents, which are vital in the adsorptive removal of MB and Cr(VI) from the aqueous solutions.

Fig. 8a illustrates the FT-IR spectra of PAS and it is composed of more number of absorption peaks. A broad band observed in the region around 3374 1/cm was easily recognized by the functional group, O—H stretching of the hydroxyl groups. The peak observed at 2924 1/cm was attributed to the asymmetric C—H stretching of methyl groups that usually occur in lignin structure from the *Pterospermum acerifolium* shells. The distinct peak at 1622 1/cm corresponds to C═C stretching vibration in aromatic rings, while the presence of nitro group N═O is indicated by the peak appeared at 1252 1/cm. The peak observed at 1044 1/cm represents the C—O stretching vibrations [47]. The band observed at 614 1/cm is assigned to the disulfides stretching (S—S). The FT-IR spectra of SPAS showed a broad band near 3195 1/cm assigned to the O—H stretching, related to hydroxyl groups and found disappeared in case of the PPAS FT-IR spectra. Similar to the PAS, the peak appeared at 2924 1/cm in case of PPAS and absent in SPAS assigned to C—H group. Both SPAS and PPAS showed peak around 1750 1/cm, attributed to the stretching vibration C═O group [48]. Peaks were observed near to 1609 1/cm and 1671 1/cm in the SPAS and PPAS, which indicate the presence of C═C stretching vibration even after the pretreatment of PAS. A peak was noted at 1223 1/cm and indicated the occurrence of nitro group in SPAS, which is also found in PAS and not present in PPAS. The comparison of the FT-IR spectra of PAS, SPAS, and PPAS revealed that major changes in the intensities of the bands were observed. Large numbers of peaks were present in the PAS, followed with SPAS, while the PPAS showed the least number of peaks. The obtained results of the SPAS and PPAS might be due to the disappearance of weak bond under the pretreatment and carbonization conditions.

4.9. Reusability of adsorbents

The reusability of adsorbents produced toward the removal of MB and Cr(VI) is an important selection factor for a superior adsorbent. The adsorption efficiency of PAS, SPAS, and PPAS for MB and Cr(VI) in the successive regeneration cycles are shown in Fig. 9. To fulfill the reuse criteria of the adsorbents, eluants of 0.1 N HCl and 0.1 N NaOH are subjected. The MB removal efficiency of PAS, SPAS, and PPAS in the third recycle are 60.62% (0.1 N HCl), 54.00% (0.1 N NaOH), 70.75% (0.1 N HCl), 55.62% (0.1 N NaOH), 89.00% (0.1 N HCl), and 78.37% (0.1 N NaOH), respectively. The results of recycle adsorption performed with 0.1 N HCl eluting agent are comparable to the original adsorption efficiency of the PAS (94.37%), SPAS (96.79%), and PPAS (99.66%) for MB removal. The third recycle for the Cr(VI) removal efficiency of PAS, SPAS, and PPAS are 28.63% (0.1 N HCl), 48.47% (0.1 N NaOH), 63.84% (0.1 N HCl), 73.18% (0.1 N NaOH), 70.90% (0.1 N HCl), and 79.95% (0.1 N NaOH), respectively. The recycle adsorption carried out using

0.1 N NaOH eluting agent are as good as to the original Cr(VI) removal efficiency by the PAS (59.71%), SPAS (83.26%), and PPAS (94.62%). The results of PAS, SPAS, and PPAS indicated their reuse without major loss of adsorption efficiency, which is important to minimize the cost investment for the large-scale application.

5. Conclusion

Adsorbents prepared from the *Pterospermum acerifolium* shells were examined for the sequestration of MB and Cr(VI) from synthetic wastewater. The removal efficiencies and adsorption capacities are significantly influenced by the parameters of initial solution pH, adsorbent dosage, initial adsorbate concentration, and temperature. Langmuir isotherm model presented better fitted with the adsorption equilibrium data than the other models considered in the present study. When compared with other adsorbents reported in the literature, the present explored adsorbents demonstrated better uptake capacity for MB (Fig. 10a) and Cr(VI) (Fig. 10b) adsorption. The kinetic assessment done using different models showed that pseudo-second order kinetic model was in better agreement with the MB and Cr(VI) adsorption process. Evaluated thermodynamic parameters revealed that the adsorption process was endothermic for MB adsorption using PAS and Cr(VI) adsorption using PAS, SPAS, and PPAS, respectively. Exothermic nature for the adsorption of MB is by means of SPAS and PPAS. The adsorbents are amenable to competent reuse with better adsorption efficiency up to three consecutive cycles using eluting agents of 0.1 N HCl for MB adsorption and 0.1 N NaOH for Cr(VI) adsorption. The overall results of the present study specified that PAS, SPAS, and PPAS adsorbents are favorably used for MB and Cr(VI) removal from aqueous solutions.

Acknowledgements

The Science and Engineering Research Board, Department of Science and Technology, Government of India (No. PDF/2016/000284) are gratefully acknowledged for funding this research. The authors are thankful to the National Institute of Technology Rourkela for providing the research facility.

References

[1] S. Rangabhashiyam, E. Suganya, N. Selvaraju, Lity Alen Varghese, Significance of exploiting non-living biomaterials for the biosorption of wastewater pollutants, World J. Microbiol. Biotechnol. 30 (2014) 1669–1689.
[2] M. Goswami, P. Phukan, Enhanced adsorption of cationic dyes using sulfonic acid modified activated carbon, J. Environ. Chem. Eng. 5 (2017) 3508–3517.
[3] S.S. Kumar, P. Balasubramanian, G. Swaminathan, Degradation potential of free and immobilized cells of white rot fungus *Phanerochaete chrysosporium* on synthetic dyes, Int. J. ChemTech Res. 5 (2013) 565–571.
[4] M.T. Yagub, T.K. Sen, H.M. Ang, Equilibrium, kinetics, and thermodynamics of methylene blue adsorption by pine tree leaves, Water Air Soil Pollut. 223 (2012) 5267–5282.
[5] J.Z. Guo, B. Li, L. Liu, K. Lv, Removal of methylene blue from aqueous solutions by chemically modified bamboo, Chemosphere 111 (2014) 225–231.
[6] V.K. Garg, M. Amita, R. Kumar, R. Gupta, Basic dye (methylene blue) removal from simulated wastewater by adsorption using Indian Rosewood sawdust: a timber industry waste, Dyes Pigments 63 (2004) 243–250.
[7] G.O. El-Sayed, Removal of methylene blue and crystal violet from aqueous solutions by palm kernel fiber, Desalination 272 (2011) 225–232.
[8] M. Ghaedi, A. Golestani Nasab, S. Khodadoust, M. Rajabi, S. Azizian, Application of activated carbon as adsorbents for efficient removal of methylene blue: kinetics and equilibrium study, J. Ind. Eng. Chem. 20 (2014) 2317–2324.
[9] S. Shakoor, A. Nasar, Removal of methylene blue dye from artificially contaminated water using citrus limetta peel waste as a very low cost adsorbent, J. Taiwan Inst. Chem. Eng. 66 (2016) 154–163.
[10] M.T. Uddin, M. Rukanuzzaman, M.M. Rahman Khan, M.A. Islam, Adsorption of methylene blue from aqueous solution by jackfruit (*Artocarpus heteropyllus*) leaf powder: a fixed-bed column study, J. Environ. Manag. 90 (2009) 3443–3450.
[11] R.A. Kristanti, M.K.A. Kamisan, T. Hadibarata, Treatability of methylene blue solution by adsorption process using *Neobalanocarpus hepmii* and *Capsicum annuum*, Water Air Soil Pollut. 227 (2016) 134.
[12] S. Rangabhashiyam, E. Suganya, Alen Varghese Lity, N. Selvaraju, Equilibrium and kinetics studies of hexavalent chromium biosorption on a novel green macroalgae *Enteromorpha* sp, Res. Chem. Intermed. 42 (2016) 1275–1294.
[13] C.C. Kan, A.H. Ibe, K.K.P. Rivera, R.O. Arazo, M.D.G. de Luna, Hexavalent chromium removal from aqueous solution by adsorbents synthesized from groundwater treatment residuals, Sustain. Environ. Res. (2017)https://doi.org/10.1016/j.serj.2017.04.001.
[14] S. Rangabhashiyam, N. Anu, N. Selvaraju, Equilibrium and kinetic modeling of chromium (VI) removal from aqueous solution by a novel biosorbent, Res. J. Chem. Environ. 18 (2014) 30–36.
[15] A. Hosseini-Bandegharaei, M.S. Hosseini, M. Sarw-Ghadi, S. Zowghi, E. Hosseini, H. Hosseini-Bandegharaei, Kinetics, equilibrium and thermodynamic study of Cr(VI) sorption into toluidine blue o-impregnated XAD-7 resin beads and its application for the treatment of wastewaters containing Cr(VI), Chem. Eng. J. 160 (2010) 190–198.
[16] D. Pathania, S. Sharma, P. Singh, Removal of methylene blue by adsorption onto activated carbon developed from *Ficus carica* bast, Arab. J. Chem. 10 (2017) S1445–S1451.
[17] S. Rangabhashiyam, N. Selvaraju, Adsorptive remediation of hexavalent chromium from synthetic wastewater by a natural and $ZnCl_2$ activated *Sterculia guttata* shell, J. Mol. Liq. 207 (2015) 39–49.
[18] I. Ozdemir, M. Sahin, R. Orhan, M. Erdem, Preparation and characterization of activated carbon from grape stalk by zinc chloride activation, Fuel Process. Technol. 125 (2014) 200–206.
[19] E. Yagmur, M. Ozmak, Z. Aktas, A novel method for production of activated carbon from waste tea by chemical activation with microwave energy, Fuel 87 (2008) 3278–3285.
[20] A. Abdolali, W.S. Guo, H.H. Ngo, S.S. Chen, N.C. Nguyen, K.L. Tung, Typical lignocellulosic wastes and by-products for biosorption process in water and wastewater treatment: a critical review, Bioresour. Technol. 160 (2014) 57–66.
[21] D. Preety, C. Kailash, P.K. Mohd, A.S. Jawed, T. Deepshikha, T.N. Florence, C. Naibedya, M. Rakesh, Phytoceramides and acylated phytosterol glucosides from *Pterospermum acerifolium* Willd. seed coat and their osteogenic activity, Phytochemistry 81 (2012) 117–125.
[22] P. Manisha, B. Nasreen, D. Preety, K.S. Vishal, K. Padam, M. Rakesh, M.B. Shailja, Immunosuppressive activity of hexane and ethanolic extracts of *Pterospermum acerifolium* seeds in BALB/c mice, Med. Chem. Res. 20 (2011) 1667–1673.
[23] S. Rangabhashiyam, N. Anu, M.S. Giri Nandagopal, N. Selvaraju, Relevance of isotherm models in biosorption of pollutants by agricultural byproducts, J. Environ. Chem. Eng. 2 (2014) 398–414.
[24] I. Langmuir, The adsorption of gases on plane surfaces of glass, mica and platinum, J. Am. Chem. Soc. 40 (1918) 1361–1403.
[25] H. Freundlich, W. Helle, On adsorption in solution, J. Am. Chem. Soc. 61 (1939) 2228–2230.
[26] G. Halsey, Physical adsorption on nonuniform surfaces, J. Chem. Phys. 16 (1948) 931–937.
[27] D.S. Jovanovic, Physical adsorption of gases I: isotherms formonolayer and multilayer adsorption, Colloid Polym. Sci. 235 (1969) 1203–1214.
[28] M. Arabloo, M.H. Ghazanfari, D. Rashtchian, Spotlight on kinetic and equilibrium adsorption of a new surfactant onto sandstone minerals: a comparative study, J. Taiwan Inst. Chem. Eng. 50 (2015) 12–23.
[29] A.N. Frumkin, Electrocapillary curve of higher aliphatic acids and the state equation of the surface layer, Int. J. Res. Phys. Chem. Chem. Phys. 116 (1925) 466–488.
[30] A.V. Kiselev, Vapor adsorption in the formation of adsorbate molecule complexes on the surface, Kolloid Zhur. 20 (1958) 338–348.
[31] B. Tang, Y. Yao, W. Chen, X. Chen, F. Zou, X. Wang, Kinetics of dyeing natural protein fibers with silver nanoparticles, Dyes Pigments 148 (2018) 224–235.
[32] S. Lagergren, About the theory of so-called adsorption of soluble substances, K. Svenska Vetenskapsakad. Handl. 24 (1898) 1–39.
[33] G. Blanchard, M. Maunaye, G. Martin, Removal of heavy metals from waters by means of natural zeolites, Water Res. 18 (1984) 1501–1507.
[34] Y.S. Ho, G. McKay, Pseudo-second order model for sorption processes, Process Biochem. 34 (1999) 451–465.
[35] F.C. Wu, R.L. Tseng, R.S. Juang, Characteristics of Elovich equation used for the analysis of adsorption kinetics in dye-chitosan systems, Chem. Eng. J. 150 (2009) 366–373.
[36] W.J. Weber, J.C. Morris, Advances inwater pollution research: removal of biologically resistant pollutants from waste waters by adsorption, Proceedings of International Conference on Water Pollution Symposium, 2, Pergamon Press, Oxford 1962, pp. 231–266.
[37] S. Rangabhashiyam, P. Balasubramanian Sujata Lata, Biosorption characteristics of methylene blue and malachite green from simulated wastewater onto *Carica papaya* wood biosorbent, Surf. Interfaces (2017)https://doi.org/10.1016/j.surfin.2017.09.011.
[38] Y. Sun, Q. Yue, B. Gao, Y. Gao, Q. Li, Y. Wang, Adsorption of hexavalent chromium on *Arundo donax Linn* activated carbon amine-crosslinked copolymer, Chem. Eng. J. 217 (2013) 240–247.
[39] Z.L.G. Wang, K. Zhai, C. He, Q. Li, P. Guo, Methylene blue adsorption from aqueous solution by loofah sponge-based porous carbons, Colloids Surf. A Physicochem. Eng. Asp. (2017)https://doi.org/10.1016/j.colsurfa.2017.10.046.
[40] R. Khosravi, M. Fazlzadehdavil, B. Barikbin, A. Akbar Taghizadeh, Removal of hexavalent chromium from aqueous solution by granular and powdered *Peganum Harmala*, Appl. Surf. Sci. 292 (2014) 670–677.
[41] G.B. Oguntimein, Biosorption of dye from textile wastewater effluent onto alkali treated dried sunflower seed hull and design of a batch adsorber, J. Environ. Chem. Eng. 3 (2015) 2647–2661.
[42] C. Carvalho dos Santos, R. Mouta, M. Carvalho Castro Junior, S. Aparecida Abreu Santana, H. Antonio dos Santos Silva, C. Wellington Brito Bezerra, Chitosan-edible oil based materials as upgraded adsorbents for textile dyes, Carbohydr. Polym. 180 (2018) 182–191.

[43] Y. Yi, J. Lv, N. Zhong, G. Wu, Biosorption of Cu^{2+} by a novel modified spent *Chrysanthemum*:kinetics, isotherm and thermodynamics, J. Environ. Chem. Eng. 5 (2017) 4151–4156.
[44] E. Daneshvar, A. Vazirzadeh, A. Niazi, M. Sillanpaa, A. Bhatnagar, A comparative study of methylene blue biosorption using different modified brown, red and green macroalgae — effect of pretreatment, Chem. Eng. J. 307 (2017) 435–446.
[45] G.M. Figueroa-Torres, M.T. Certucha-Barragan, E. Acedo-Felix, O. Monge-Amaya, F.J. Almendariz-Tapia, L.A. Gasca-Estefania, Kinetic studies of heavy metals biosorption by acidogenic biomass immobilized in clinoptilolite, J. Taiwan Inst. Chem. Eng. 61 (2016) 241–246.
[46] G. Markou, D. Mitrogiannis, A. Celekli, H. Bozkurt, C.V. Chrysikopoulos, Biosorption of Cu^{2+} and Ni^{2+} by *Arthrospira platensis* with different biochemical compositions, Chem. Eng. J. 259 (2015) 806–813.
[47] M. Smilja, S. Ana, L. Zorica, L. Slavica, S. Mirjana, U. Dragan, Application of raw peach shell particles for removal of methylene blue, J. Environ. Chem. Eng. 3 (2015) 716–724.
[48] Z.K. George, A.D. Eleni, A.M. Kostas, Activated carbons produced by pyrolysis of waste potato peels: cobalt ions removal by adsorption, Colloids Surf. A Physicochem. Eng. Asp. 490 (2016) 74–83.
[49] M.S. Ur Rehman, I. Kim, J.I. Han, Adsorption of methylene blue dye from aqueous solution by sugar extracted spent rice biomass, Carbohydr. Polym. 90 (2012) 1314–1322.
[50] M. Ertas, B. Acemioglu, M. Hakki Alma, M. Usta, Removal of methylene blue from aqueous solution using cotton stalk, cotton waste and cotton dust, J. Hazard. Mater. 183 (2010) 421–427.
[51] S. Banerjee, R. Kumar Gautam, P. Rai, Mahesh Chandra Chattopadhyaya, Adsorptive removal of toxic dyes from aqueous phase using notorious weed *Lantana camara* (Linn.) as biosorbent, Res. Chem. Intermed. 42 (2016) 5677–5708.
[52] J.O. Amode, J.H. Santos, Z.M. Alam, A.H. Mirza, C.C. Mei, Adsorption of methylene blue from aqueous solution using untreated and treated (*Metroxylon* spp.) waste adsorbent: equilibrium and kinetics studies, Int. J. Ind. Chem. 7 (2016) 333–345.
[53] B.H. Hameed, A.A. Ahmad, Batch adsorption of methylene blue from aqueous solution by garlic peel, an agricultural waste biomass, J. Hazard. Mater. 164 (2009) 870–875.
[54] M.K. Dahri, M.R.R. Kooh, L.B.L. Lim, Water remediation using low cost adsorbent walnut shell for removal of malachite green: equilibrium, kinetics, thermodynamic and regeneration studies, J. Environ. Chem. Eng. 2 (2014) 1434–1444.
[55] R. Gottipati, S. Mishra, Preparation of microporous activated carbon from *Aegle Marmelos* fruit shell and its application in removal of chromium(VI) from aqueous phase, J. Ind. Eng. Chem. 36 (2016) 355–363.
[56] A. Ali, K. Saeed, F. Mabood, Removal of chromium (VI) from aqueous medium using chemically modified banana peels as efficient low-cost adsorbent, Alex. Eng. J. 55 (2016) 2933–2942.
[57] R. Khalid, A. Abbas, W. Ahmad, N. Ramzan, Reyad Shawabkeh, Adsorptive potential of *Acacia Nilotica* based adsorbent for chromium (VI) from an aqueous phase, Chin. J. Chem. Eng. (2017)https://doi.org/10.1016/j.cjche.2017.08.017.
[58] Z.A. AL-Othman, R. Ali, M. Naushad, Hexavalent chromium removal from aqueous medium by activated carbon prepared from peanut shell: adsorption kinetics, equilibrium and thermodynamic studies, Chem. Eng. J. 184 (2012) 238–247.
[59] H. Liu, S. Liang, J. Gao, H.H. Ngo, W. Guo, Z. Guo, J. Wang, Y. Li, Enhancement of Cr (VI) removal by modifying activated carbon developed from *Zizania caduciflora* with tartaric acid during phosphoric acid activation, Chem. Eng. J. 246 (2014) 168–174.
[60] A. Kumar, H.M. Jena, Adsorption of Cr(VI) from aqueous solution by prepared high surface area activated carbon from Fox nutshell by chemical activation with H_3PO_4, J. Environ. Chem. Eng. 5 (2017) 2032–2041.
[61] S. Kuppusamy, P. Thavamani, M. Megharaj, K. Venkateswarlu, Y.B. Lee, R. Naidu, Potential of *Melaleuca diosmifolia* leaf as a low-cost adsorbent for hexavalent chromium removal from contaminated water bodies, Process. Saf. Environ. Prot. 100 (2016) 173–182.